Hindawi
Advances in Civil Engineering
Volume 2020, Article ID 8820172, 12 pages
https://doi.org/10.1155/2020/8820172

Research Article

Physics and Dynamics Characteristics and Energy Analysis of Freeze-Thaw Limestone

Qi Ping,[1,2,3] **Hongjian Sun**,[1,2,3] **Chuanliang Zhang**,[1,2,3] **and Xin Zhou**[2,3]

[1]*State Key Laboratory of Mining Response and Disaster Prevention and Control in Deep Coal Mine, Anhui University of Science and Technology, Huainan, Anhui 232001, China*
[2]*Research Center of Mine Underground Engineering, Ministry of Education, Anhui University of Science and Technology, Huainan, Anhui 232001, China*
[3]*School of Civil Engineering and Architecture, Anhui University of Science and Technology, Huainan, Anhui 232001, China*

Correspondence should be addressed to Qi Ping; ahpingqi@163.com

Received 30 April 2020; Revised 4 June 2020; Accepted 5 June 2020; Published 24 June 2020

Academic Editor: Hang Lin

In order to study the physical and dynamic properties of rock after damage, an open-type saturated water freeze-thaw test at ±20°C was carried out on the limestone specimen, the size, quality, and longitudinal wave velocity with measured after freeze-thaw cycles for 0, 10, 20, 30, 40, 50, 60, 70, 80, 90, and 100 times, and the SHPB test device was used to carry out the impact compression test with eight kinds of loading rate. This text analyzes the damage evolution characteristics on the physical properties of limestone of cycle times of freeze-thaw and discusses the dynamic compression mechanical characteristics and energy dissipation law of limestone specimens after freeze-thaw cycles. The test results show that the mass and longitudinal wave velocity of the specimen decreased and the volume and density increased. The damage factors have the quadratic function positive correlation with the cycle time of freeze-thaw. Moreover, the dynamic compression stress-strain curves of the specimens under different loading rates are similar in shape, and the curve shows an upward trend with increasing loading speed. In addition, with the loading rate increasing, the dynamic compressive strength and dynamic elastic modulus of the specimen increased and the dynamic strain decreased. In the SHPB test, the reflected energy, transmitted energy, and absorbed energy all increased linearly with incident energy. The dynamic compressive strength and absorbed energy increase as a power function, and the strain rate and absorbed energy increase as a quadratic function.

1. Introduction

There are different styles of climate and environment on Earth. The coverage of permafrost, seasonal frozen soil, and short-term frozen soil is about 50% of the land area, and the distribution of frozen soil on the Earth has latitude zonality and altitude zonality. However, in China, even though the region is vast and the climate is diverse, the frozen soil area still accounts for more than 70% of the total territory, of which seasonal frozen soil accounts for half of the total land area, which is generally distributed in the low latitude or low temperature area, while the permafrost is distributed in the northeast, the western mountain plateau, and some higher mountains in the East (Changbai Mountain, Taibai Mountain and Wutai Mountain). When carrying out resource development and engineering construction in these areas, we have to take into account the special geological conditions of frozen soil area, generally such as the rock slope, positive temperature gas transmission pipeline, tunnel, foundation, etc. [1], especially with the national western development and the transfer of strategic center in recent years. The engineering construction is developing day by day, so it is very urgent for us to recognize the rock and soil mass in the frozen soil area.

Frozen soil generally refers to various geotechnical and soil containing ice [2], whose temperature is at or below 0°C. Among that, the soil is the accumulation of rock formed by the various handling effects after natural weathering, but the rock is a naturally produced mineral or glass aggregate with a stable appearance, combined in a certain way. The difference

between rock and soil is that rock mineral particles have a strong connection (crystalline connection, cemented connection), which is not only an important structural feature of the rock but also the main feature to distinguish it from the soil, giving it excellent engineering geological properties. However, the soil lacks such a connection or is weakly connected between particles. Rock has the characteristics of high strength, difficult deformation, integrity, and good water resistance. But it also has defects when used as the foundation or building environment, namely, its weak plane which can cause breaking up when it is cut, damaging its integrity resulting in poor and uneven physical and mechanical properties, so the rock (body) structure is far more complicated than the soil. In other words, rocks have strong anisotropy, heterogeneity, discontinuity, and complexity. Compared with rocks, soil can be regarded as continuous, uniform, and isotropic materials and media. Research on the mechanics of frozen soil is earlier than that of frozen rock. But in recent years, with the increasing demand for engineering, the general frozen soil mechanics is no longer suitable for the study of frozen rock. This is bound to make the frozen rock problem a new problem to explore the idea; the effect of freeze-thaw on rock damage expansion is actually very complicated. Different freezing temperatures and freezing speeds have different effects on the mechanical properties of different types of rock materials. The freeze-thaw cycle is the main factor for the freeze-thaw damage expansion of rocks [3].

In cold regions, due to seasonal climate change and temperature change, the physical and mechanical properties of rocks have changed under the action of freeze-thaw cycles. As China continues to increase the construction in frozen rock areas in the process of western development [4], such as the Tamu Basin Sebei-Xining-Lanzhou Gas Pipeline, Qinghai-Tibet Railway, South-to-North Water Transfer Project, and West-East Power Transmission Project, the rock mass is lifted and lowered around the freezing point one or more times under the disturbance of the external environment, which causes the internal continuous freezing and melting of the rock mass, which is an important factor affecting the safety and stability of the engineering. Therefore, it is of important significance to study the mechanical and physical characteristics of rock mass in the frozen region under the action of freeze-thaw cycles for engineering construction, resource development and utilization, and economy.

At present, when studying the characteristics of rock mass under freeze-thaw cycles, static loads are generally used, and dynamic mechanical characteristics of rocks are less studied. Among them, the mechanical characteristics of rocks under different cycle temperatures, cycle times, and cycle times are studied more, while from a certain cycle temperature to normal temperature, the effect of freeze-thaw cycles on the rock is less studied. Due to blasting, excavation, and dynamic loads affected by natural factors during the construction of open-air engineering, this article aims to study the mechanical properties of rocks in SHPB dynamic impact compression tests under certain freeze-thaw cycles and different strain rates, which is of great significance for cold area engineering.

At present, a lot of work has been done at home and abroad on the study of physical and mechanical characteristics of rock under freeze-thaw conditions. PARK et al. [5] used diorite, basalt, and tuff as specimens to maintain saturation and studied the changes in the internal microstructure of the rock during repeated freeze-thaw cycles; Khalari et al. [6] performed freeze-thaw, dry-wet, cold-heat cycle tests on sandstones, measured longitudinal wave velocity, porosity, and uniaxial compression strength and analyzed physical and mechanical properties of the rock specimens. Martínez-Martínez [7] carried out tests on a series of changes in wave speed, intensity, porosity, etc. on carbonate rock specimens after 100 freeze-thaw cycles. Deng et al. [8] further researched the effects of freeze-thaw weathering on sandstone damage from the perspective of energy analysis. Liu et al. [9] used NMR technology to study the damage evolution law of rocks with macrodefects and microdefects in the freeze-thaw cycles. Yang Niange et al. [10] studied the dynamic characteristics and failure law of sandstone under the freeze-thaw cycles and revealed the mechanism of freeze-thaw damage. Lei et al. [11] analyzed the relationship with dynamic load strength, strain rate, and freeze-thaw cycles in granite-porphyry. Hailiang et al. [12] carried out a study on the damage model of saturated sandstone under freeze-thaw cycles. Yang et al. [13] clarified the freeze-thaw damage identification methods and damage mechanisms under different scale conditions.

In the above results, the SHPB test is more common for different numbers of cycles and the same strain rate of rock specimens under freeze-thaw cycles [14]. Considering the effects of dynamic characteristics of different strain rates under certain freeze-thaw cycles, there are fewer experimental studies.

In this paper, to freeze-thaw cycles test of −20°C~+20°C on limestone from Bagong Mountain, Huainan, Anhui was carried out, performing the static and dynamic load mechanics experiments on rock specimens before and after freezing and thawing. Research on the regularity of the dynamic performance and physical properties of the vehicle was also carried out, exploring the forms of dynamic failure and providing research ideas and methods for the dynamic disturbance of rocks in the cold region under the freeze-thaw cycles.

2. Test Design

2.1. Sample Preparation. Limestone with good granularity and uniformity was selected as the specimen. In order to compare the dynamic and static load test strength and reduce the end effect and inertial effect of the specimens [15], the specimens were uniformly processed into a 25 mm height and 50 mm diameter Cylinder. All specimens are ground at both ends. The allowable deviation of the unevenness of the two end faces is ±0.05 mm. The end face should be perpendicular to the axis of the test piece, and the allowable deviation is ±0.25°.

2.2. Test Equipment. Related equipment of freeze-thaw test: TEST-1000 Freezing Chamber whose working room is 1000 mm × 1000 mm × 1000 mm, the temperature range to −60°C~150°C, 101-3A electric blast constant temperature

drying oven, C61 nonmetal ultrasonic detector, electronic balance, dryer, test piece saturation equipment, and static mechanics experimental system (RMT-150B), which are frozen in water and dissolved in water protocol to perform freeze-thaw tests.

The impact test of the rock specimen used the Hopkinson pressure bar test device (SHPB) of the State Key Laboratory of Mining Response and Disaster Prevention and Control of Deep Coal Mine of Anhui University of Science and Technology to study the dynamic response characteristics of the rock. The device is composed of a stress generating device, a stress propagation mechanism, a stress absorption device, an axial pressure system, a confining pressure system, and a data acquisition system. The device's punch, incident rod, transmission rod, and absorption rod are made of 40Cr alloy steel. Poisson's ratio is 0.28, the elastic wave velocity is 5380 mm/s, the diameter of the incident rod and the transmission rod are 50 mm, the length is 2000 mm and 1500 mm, respectively, using a spindle punch, and the data acquisition and display equipment is SDY2107A super dynamic strain gauge and DL850E oscilloscope.

2.3. Text Method. According to the relevant specifications and test conditions, the test piece is first placed in an oven, and then it is baked at 105°C to 110°C for 24 hours, taken out, and put in a dryer to cool to room temperature and then weighed. Then, the free immersion method was used to saturate the test block by freely absorbing water in for 48 hours, and the relevant physical parameters were measured. The single cycle of rock freeze-thaw cycle is 8 h, that is, put the saturated test piece into the storage box, then put it in the freezing chamber (Figure 1), and freeze it at −20°C ± 2°C for 4 h. Then remove the test piece and put it in the water-filled temperature box. In the water temperature box, keep the water temperature at 20°C ± 2°C to dissolve for 4 h, which is one freeze-thaw cycle [16]. The relationship between cycle temperature and time is shown in Figure 2.

The test is divided into 8 groups according to the impact pressure, and 100 freeze-thaw cycles are performed. The SHPB device was used after the cycles (shown in Figure 3) to do the text impact pressure. The impact pressures are 0.3 MPa, 0.325 MPa, 0.35 MPa, 0.375 MPa, 0.4 MPa, 0.425 MPa, 0.45 MPa, and 0.475 MPa, 4 of which are a group to be used to test rocks for dynamic mechanical properties.

The mass, size, wave velocity, and density of rock specimen were measured after every 10 freeze-thaw cycles. Before the impact test, a static test on the specimen was performed, measuring its uniaxial compressive strength. The incident wave, transmitted wave, and reflected waveform of the specimen under different impact pressures were recorded during the dynamic impact test, which is convenient for the dynamic stress-strain curve fitting in the later.

3. Physical Properties and Damage Ratio of Freeze-Thaw Saturated Rock

3.1. Damage Ratio Morphology of Freeze-Thaw Saturated Rocks. Figure 4 is a typical photo of saturated limestone after the freeze-thaw cycles. It was found that the damage ratio morphology of saturated limestone mainly manifested as changes in the water molecule morphology inside the rock specimen, which weakened the connection between the surface particles after 20 freeze-thaw cycles and were accompanied by the generation of microfissures. After 60 cycles of freeze-thaw cycles, the limestone surface began to fall off in slices and crack propagation increasingly. After 100

Figure 1: Freezing and thawing cycle test freezing room.

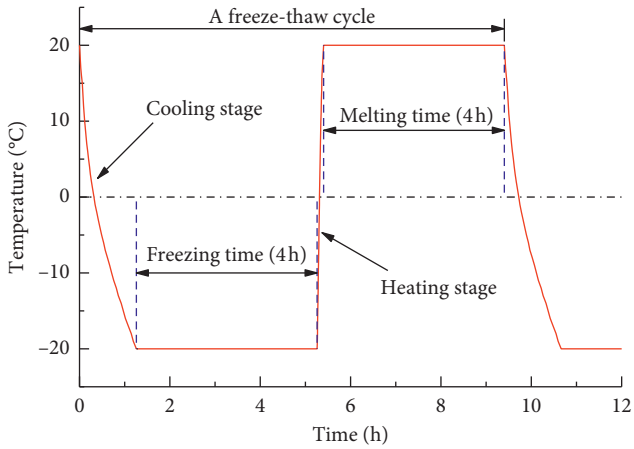

Figure 2: Cycle temperature and time.

Figure 3: SHPB device.

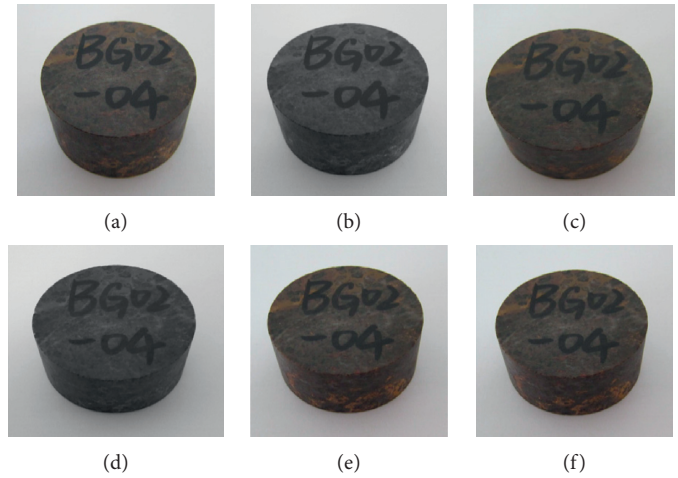

Figure 4: Morphology of rock freezing and thawing: (a) 0 F-T cycles, (b) 20 F-T cycles, (c) 40 F-T cycles, (d) 60 F-T cycles, (e) 80 F-T cycles, and (f) 100 F-T cycles.

freeze-thaw cycles, severe individual specimens fracture along the bedding. This phenomenon is due to the uneven expansion of the pore inside the rock specimen under the continuous ice-water transformation of pore water, causing the internal fractures to continuously expand and develop along the frail belt of the rocks, eventually causing the rock samples to converge and expand along the bedding fractures, and eventually run through the rock samples.

3.2. Damage Performance of Freeze-Thaw Saturated Rock. In primary materials, there is damage. With the effect of external environment and load, microfissures, microvoids, shear bands, and other mesodamaged elements in the material began to initiate, converge, and develop, and finally formed a dynamic evolution process of damage [17]. Therefore, this article selects the macro aspect as the benchmark for measuring damage, studies the damage changes of freeze-thaw saturated rocks, and reveals the damage characteristics reflected by the changes of rock macrophysical phenomena.

This article aims to use ultrasound as a medium to explore the relevant information inside saturated rocks [18]. Ultrasonic inspection is a nondestructive testing method that uses the difference in the acoustic performance of the material and its defects to reflect the ultrasonic propagation waveform and the energy change of the penetration time to check the internal defects of the material. Because the propagation speed of the longitudinal wave is fast, the longitudinal wave is generally used for detection.

The propagation velocity of longitudinal waves is shown in the following equation:

$$V_L = \sqrt{\frac{E}{\rho}}\sqrt{\frac{1-\mu}{(1+\mu)(1-2\mu)}},$$
$$\widetilde{V}_L = \sqrt{\frac{\widetilde{E}}{\widetilde{\rho}}}\sqrt{\frac{1-\mu}{(1+\mu)(1+2\mu)}}. \quad (1)$$

In the formula, μ is Poisson's ratio of the continuous medium material (assuming the material is isotropic and Poisson's ratio of the material does not change with damage), E and ρ are the elastic modulus and density of the saturated rock in the nondamaged state, $\widetilde{E}$ and $\widetilde{\rho}$ are the elastic modulus and density of the damaged material, and the volume change caused by the two-phase conversion of water and ice under the conditions of freeze-thaw cycle leads to the expansion of microfissures, which leads to the macroscopic physical deterioration of performance. Elastic modulus is generally used to quantify the degree of damage. The damage formula is shown in the following equation:

$$D = 1 - \frac{\widetilde{E}}{E}. \quad (2)$$

Bringing the longitudinal wave velocity formula into the following, we obtain

$$D = 1 - \frac{\widetilde{\rho}}{\rho}\frac{\widetilde{v}_L^2}{v_L^2}. \quad (3)$$

When D is small, a in the formula can be approximately equal to 1, so it can be assumed that

$$D = 1 - \frac{\widetilde{v}_L^2}{v_L^2}. \quad (4)$$

After 100 freeze-thaw cycles, the damage changes caused by the average wave velocity of the 8 groups of saturated rock specimens are shown in Table 1.

It can be seen from Table 1 that with the increase of the number of freeze-thaw cycles, the damage degree of saturated limestone continues to increase, and various mineral crystals within the rock are distorted by the water-ice two-phase disturbance, resulting in the expansion of the initial fractures, as well as the damage of the interface of the crystal particles, and finally various cracks were generated around the crystal grains. It is precise because of the freeze-thaw cycle that the microcracks inside the rock sample continued to develop, resulting in changes in the macrophysical

Table 1: Rock damage variables and freeze-thaw times.

Specimen groups	Number of freeze-thaw cycles										
	0	10	20	30	40	50	60	70	80	90	100
D1	0	0.18	0.18	0.18	0.18	0.18	0.27	0.31	0.31	0.38	0.38
D2	0	0.20	0.27	0.20	0.29	0.33	0.29	0.33	0.36	0.40	0.40
D3	0	0.10	0.21	0.25	0.25	0.29	0.29	0.33	0.36	0.46	0.43
D4	0	0.18	0.31	0.28	0.31	0.37	0.31	0.31	0.36	0.41	0.46
D5	0	0.08	0.20	0.27	0.21	0.27	0.27	0.26	0.27	0.33	0.43
D6	0	0.15	0.26	0.19	0.32	0.32	0.32	0.32	0.37	0.42	0.37
D7	0	0.17	0.24	0.21	0.20	0.33	0.21	0.27	0.33	0.34	0.38
D8	0	0.20	0.23	0.20	0.33	0.33	0.33	0.43	0.38	0.38	0.42

properties of the rock sample, such as the continuous attenuation of the longitudinal wave velocity. However, at the late stage of the freeze-thaw cycle, due to the weakening effect of freeze-thaw, the growth rate of the damage variable has decreased [19].

3.3. Mass Changes of Freezing and Thawing Saturated Rock. It can be seen from Figure 5 that after 100 freeze-thaw cycles, the average saturation mass increase rate ($\overline{M}_r$) of each group has an obvious correlation characteristic of the number of freeze-thaw cycles, and it increases with the increase of the number of freeze-thaw cycles. The cubic function increases and its fitting formula is shown in the following equation:

$$\overline{M}_r = 4.37E^{-7}N^3 - 9.06E^{-5}N^2 + 0.00665N - 2.51748. \quad (5)$$

The relative coefficient is $R^2 = 0.996$, and the basic changes are as follows:

(1) In the first 40 freeze-thaw cycles, the increase rate of the mass of the average saturated water almost increased linearly, and the increase rate was relatively large, reaching 0.096%. Due to the initial stage of the freeze-thaw cycle test, the frost expansion force generated by the continuous conversion of the two water phases causing the rock sample cracks to continue to expand and increase, and the initiation of new cracks, the internal cracks in the rock sample expands faster. During the melting process, the external water continuously migrated into the new fissures and became saturated again, and the water content of the rock sample increased [20], resulting in the increasing rate of mass increase.

(2) From the 50th to the 90th freeze-thaw cycles, the average saturated water mass growth rate increases more slowly, with an increased rate of only 0.02%. This is because, during the freeze-thaw cycle, the particles on the surface of the rock specimen are peeled off due to water migration and the peeling and erosion caused by the damage, resulting in the rate of decrease in the quality of the rock specimen affects the rate of increase in the pore water content, resulting in the rock specimen, and the rate of mass increase is slower.

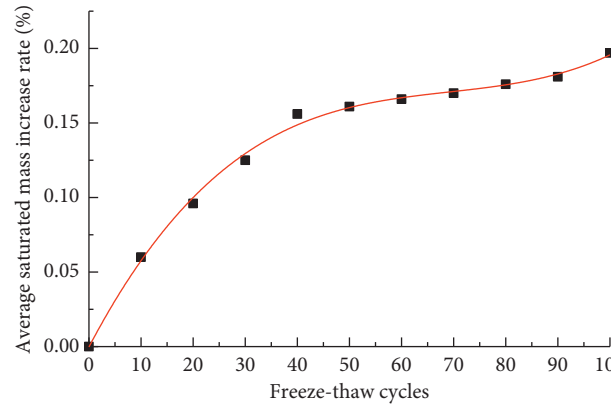

Figure 5: Change rate of average saturated water quality after different freeze-thaw cycles.

(3) In the 100th freeze-thaw cycle, the rate of increase of the rock mass sample was faster than before. This is because the impact of the rate of decrease in the quality of the rock sample on the rate of increase in pore water gradually weakens in the late freeze-thaw cycle.

3.4. Changes in Density of Freeze-Thaw Saturated Rocks. As shown in Figure 6, the average volume change rate ($\overline{V}_r$) of the rock sample is negatively correlated with the number of freeze-thaw cycles. It decreases with a cubic function as the number of freeze-thaw cycles increases. The fitting formula (6) is as follows:

$$\overline{V}_r = -6.94E^{-7}N^3 + 1.01E^{-4}N^2 - 0.0076N - 0.016. \quad (6)$$

The relative coefficient is $R^2 = 0.97365$, as can also be seen from the figure. Before the 60th freeze-thaw cycle, the average volume change rate of rock samples decreased by 0.14% and the maximum volume reduction rate was 0.24%. At the 60th to 90th freeze-thaw cycles after the second freeze-thaw cycle, the average volume change rate of the rock sample decreased by 0.18%, which was an increase compared with the previous one. After the last 100 freeze-thaw cycles, the decrease rate of the average volume change rate decreased.

As shown in Figure 7, the average saturation density ($\overline{\rho}$) of the rock sample is positively correlated with the number of freeze-thaw cycles, and it increases with a quadratic

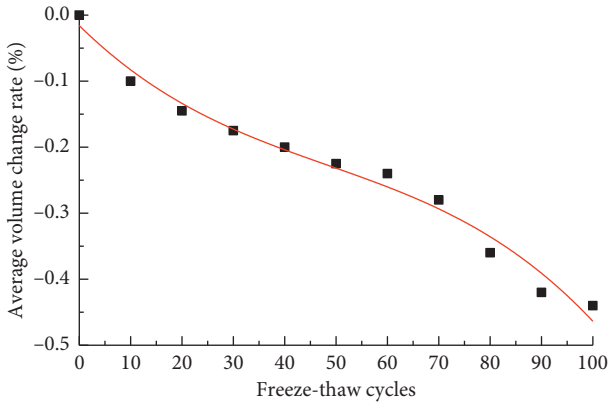

Figure 6: Average volume change rate after different freeze-thaw cycles.

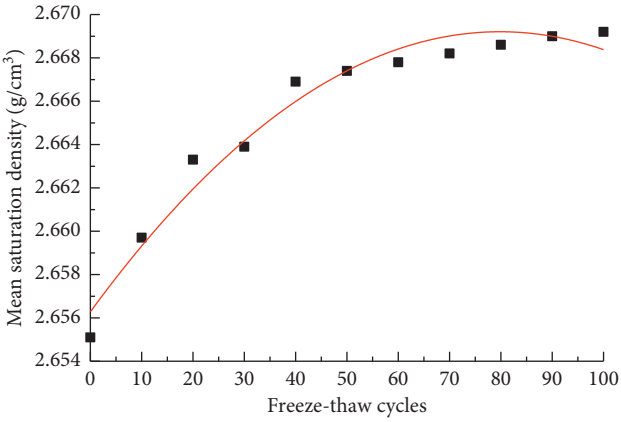

Figure 7: Changes in average saturation density under different freeze-thaw cycles.

function as the number of freeze-thaw cycles increases. The fitting formula (7) is as follows:

$$\overline{\rho} = -2.03E^{-6}N^2 + 3.24E^{-4} + 2.6563. \quad (7)$$

The relative coefficient is $R^2 = 0.96089$. It can also be seen from the figure that before 60th freeze-thaw cycle, the expansion of primary cracks and the development of new cracks due to the frost uplift and expansion caused increased water migration and increased mass, and the average volume change rate was negative. So the rock's average saturation density of the sample increased by a large margin, with a growth rate of 0.478%. After the 70th to 100th freeze-thaw cycles, the average saturation density of the rock sample increased less than before, with a growth rate of only 0.037%. This is because in the late freeze-thaw cycle, water molecules severely weakened the internal connection of the rock sample, resulting in faster and faster expansion of the fissures, and the rate of decrease in the volume of the rock sample became gradually smaller than the rate of increase in the mass of the rock sample.

3.5. Wave Velocity Changes of Freeze-Thaw Saturated Rocks. As shown in Figure 8, as the number of freeze-thaw cycles increases, the wave velocity of the average saturated rock

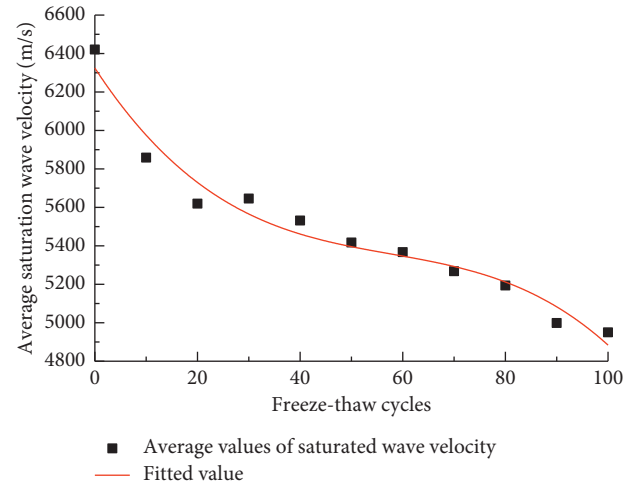

Figure 8: Variation of mean saturation wave velocity under different freeze-thaw cycles.

sample continues to decline. Both can be represented by cubic polynomial functions, and the fitting formula is as follows:

$$\overline{V} = 3.61E^{-3}N^3 + 0.625N^2 - 40.808N + 6324.532, \quad (8)$$

$\overline{V}$ is the average of the change of the average saturation of wave velocity and N is the number of cycles, and the relative coefficient between the two is $R^2 = 0.95076$. And before the 20th cycle of freezing and thawing, the wave velocity of the rock specimen had a larger decrease amplitude, of which the maximum decrease amplitude was 12.48%. This is mainly due to the large increase in pore water at the beginning of the freeze-thaw cycle, and the propagation velocity of waves in water is less than that in rocks, resulting in a significant decrease in wave propagation velocity. But after 20 times, the wave velocity decreased more slowly. This is because the increasing rate of pore water gradually became slower, and because of the continuous generation of new fissures, the wave propagation energy attenuated.

4. Mechanical Properties and Energy Dissipation of Freeze-Thaw Saturated Rocks

4.1. Dynamic Stress-Strain Curve Change Law. As shown in Figure 9, the stress-strain curve of limestone under static load is divided into consolidation process, elastic stage, yield stage, and failure stage, and the rock failure strength is 110.295 MPa, in which the consolidation process is more obvious, and the residual strength decreases faster.

As shown in Figure 10, in order to make the specimen load at near-constant strain rate before the dynamic mechanical measurement, to ensure the reliability of the SHPB test [21], the incident bar in this paper is a tapered transition variable cross-section form, which can increase the stress uniformity of the specimen [22]. And even in the postfailure stage of the specimen, it can maintain a good stress equilibrium state [23].

As shown in Figure 11, the following conclusions can be drawn from the dynamic stress-strain curve changes of limestone under different loading pressures:

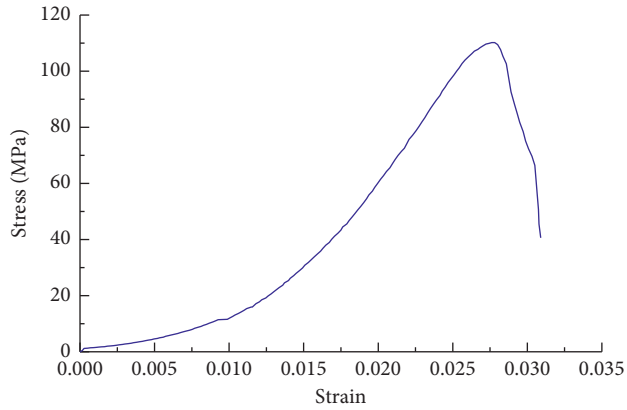

Figure 9: Stress-strain curve of limestone under static load.

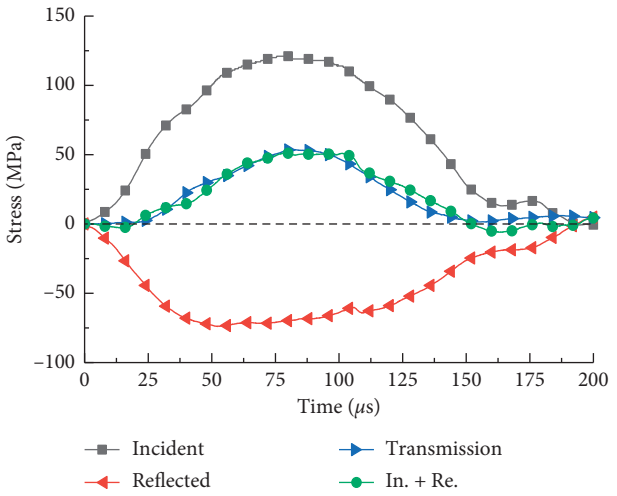

Figure 10: Stress balance diagram.

(1) As the impact pressure increases, the dynamic stress-strain curve of the rock tends to move away from the strain coordinate axis, and the elastic-plastic stage also approaches the stress coordinate axis. Also, the curves under different impact pressures show an envelope state. Under the condition of a certain number of freeze-thaw cycles, the dynamic compressive strength of rock increases with the increase of impact pressure.

(2) Compared with the limestone stress-strain curve under static load, the dynamic stress-strain curve has a smaller strain range and the maximum value is only about 0.015, only half of the static load. During the dynamic impact process, the rock specimen directly enters into the elastic stage before the consolidation process. This is because the strain rate is too fast, and the rock specimen deforms before it can be consolidated. The plastic yield stage is more obvious, and the declining trend of residual strength during the failure stage is gentler. The failure mode of rock specimen changes from brittle failure to ductile failure, and this is because although the freeze-thaw

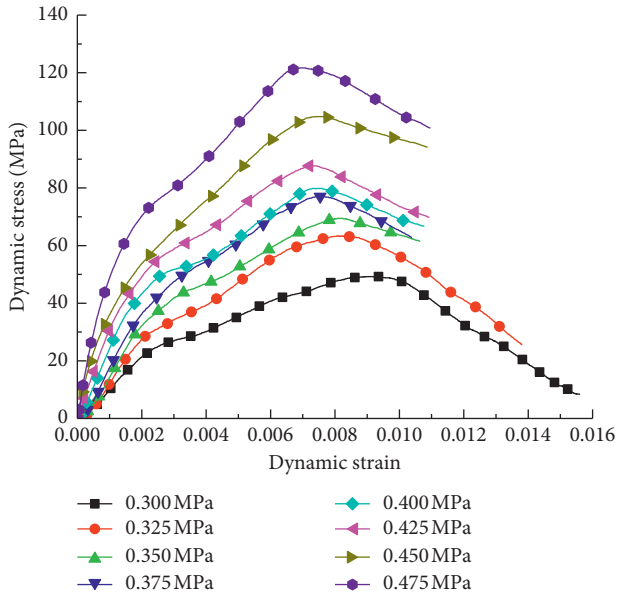

Figure 11: Dynamic stress-strain curves of limestone under different loading pressures.

experiment caused damage to the interior of the rock specimen, the expanding cracks weakened the particle connection between the rock specimens. But at the same time, it also increased the friction between the particles, and this friction leads to deformability. And as the strain rate increases, the yield stage of the rock specimen becomes longer and longer, and the unloading trend of the strain rate in the failure stage becomes more and more rapid, and the ductility characteristic is gradually blurred. This is because the force between the water molecules of the saturated rock specimen under the effect of high strain rate becomes strong, so that the friction effect between the particles gradually weakens, which leads to the weakening of ductility.

(3) As the impact pressure increases, the average strain rate of the rock specimen gradually increases. And as the dynamic elastic modulus of the rock gradually increases, the slope of the elastic phase in the stress-strain curve becomes larger and larger, and the dynamic elastic modulus of the rock specimen has a strong sensitivity [24] to the corresponding rate as shown in Figure 12.

There is a polynomial relationship between the two, and the fitting relationship is shown in the following equation:

$$E = 15.5E^{-4}\dot{\varepsilon}^2 - 0.31\dot{\varepsilon} + 22.66. \quad (9)$$

E is the dynamic elastic modulus, $\dot{\varepsilon}$ is the average strain rate, and the correlation coefficient R^2 is 0.8494. When the strain rate is less than 132.5 s^{-1}, the curve is gentler, and the dynamic elastic modulus increases more slowly. When the strain rate is greater than 132.5 s^{-1}, the curve gradually becomes steeper and the growth rate becomes faster. For the initial stage of the stress-strain curve, when the strain rate is

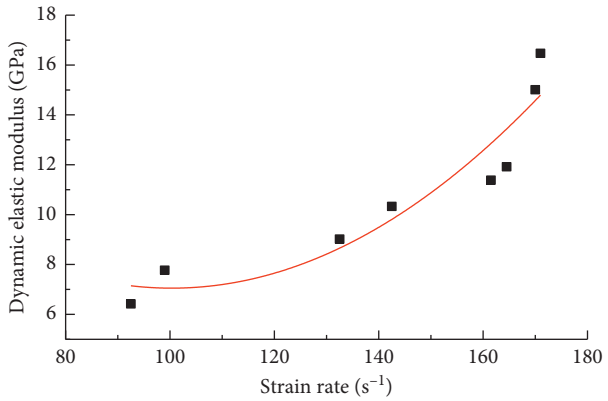

Figure 12: Dynamic elastic modulus changes of saturated limestone under different strain rates.

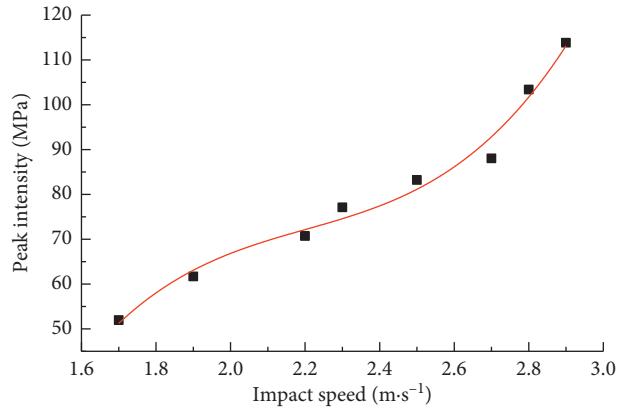

Figure 13: Changes in peak limestone intensity at different impact velocities.

lower than 164.5 s^{-1} because the rock specimen is in the comparison stage, the initial elastic modulus of the rock specimen is small. While the strain rate is higher than 164.5 s^{-1}, the initial consolidation state of the rock specimen disappeared, and it quickly approaches the elastic state.

4.2. Loading Rate and Dynamic Peak Stress. With the impact pressure increasing, the loading rate increases, and the dynamic loading strength of limestone has a significant loading rate effect. Under the condition that the number of freeze-thaw cycles is a fixed value, the dynamic peak strength generally increases with the increase of the loading rate. Rock specimens have different sensitivities to strain rate, so individual dynamic load strengths are different. We can use the cubic function mode to curve fit the curve, as shown in Figure 13.

It can be seen from Figure 13 that the fitting formula (10) is as follows:

$$\sigma = 71.95v^3 - 475.3v^2 + 1070.238v - 748.0524. \quad (10)$$

Among them, the correlation coefficient is $R^2 = 0.97559$. When the loading rate v increases from 1.7 m/s to 2.2 m/s, the peak intensity σ increases from 51.95 MPa to 70.7 MPa, with an increased amplitude of 36.09%. When the loading rate v increases from 2.3 m/s to 2.9 m/s, the corresponding peak intensity σ increases from 77.1 MPa to 113.85 MPa, with a 47.67% increase amplitude. It shows that the loading rate has a significant loading rate strengthening effect on the dynamic peak strength of the rock specimen.

The time t_M required for rock rupture is shown in the following equation:

$$t_M = (m+4)^{-1/(m+3)} \alpha^{-1/(m+3)} \dot{\varepsilon}^{-m/(m+3)}, \quad (11)$$

m and α are both constants. From the above formula, it can be seen that when the average strain rate gradually increases with the impact velocity, the rupture time of the rock gradually decreases. The great conduction relationship between the dynamic strength of the rock and the instability of the fissure expansion and the time experienced by the general rock instability expansion phase is generally one-tenth of the entire test time [25]. Since the saturated limestone has undergone 100 freeze-thaw cycles, its internal cracks are well developed. During the dynamic failure process, due to the compression deformation of the rock specimen, the pore water pressure continuously promotes the expansion of the cracks. So when the impact velocity increases, the cracks expand. The speed gradually increases, and the time required for unstable expansion is getting less and less, and even is less than the estimated failure time during the failure phase of the entire experiment, resulting in a gradual increase in peak strength, proving the dual influence of water and strain rate on strength [26]. And the excessively high impact velocity increases the probability of collision between the initial crack and the pores, making the pore water pressure gradually increase, so the increase rate of peak strength gradually went up [27, 28].

4.3. Principle of Energy Analysis of SHPB System. A natural rock contains a lot of defects, and its deformation and destruction process can be regarded as a process of continuous energy and material exchange with the external environment. The mechanical energy and heat energy of the external environment on the rock are emitted as heat energy, radiation energy, and other energy [29]. According to the one-dimensional elastic wave theory, the incident energy, reflected energy, and transmitted energy in the SHPB experiment can be obtained [30] and the following equation is obtained:

$$\left.\begin{aligned} W_I &= \left(\frac{A_b C_b}{E_b}\right) \int \sigma_I^2 d_t \\ W_R &= \left(\frac{A_b C_b}{E_b}\right) \int \sigma_R^2 d_t \\ W_T &= \left(\frac{A_b C_b}{E_b}\right) \int \sigma_T^2 d_t \end{aligned}\right\}. \quad (12)$$

A is the cross-sectional area of the test bar, C and E represent the longitudinal wave velocity and elastic modulus of the test bar. σ is the stress time history of the test bar stress wave.

According to the principle of energy conservation, the absorbed energy of the rock is shown in the following equation:

$$W_L = W_I - W_R - W_T, \tag{13}$$

$$W_L = W_{\mathrm{FD}} + W_K + W_O, \tag{14}$$

W_{FD} is the breakage energy, namely, the energy consumed by the specimen when it is crushed (proliferation and expansion of cracks inside the specimen), and W_k is the kinetic energy of the ejection, which is the energy carried by the specimen when it is broken and splashed. W_O refers to other energy consumption, such as sound energy and heat energy. Among them, ejection kinetic energy (W_k) and other energy consumption (W_O) are too little and can be ignored, and the absorption energy W_L is used instead of the breakage energy (W_{FD}), which has little effect on the results of the study [31, 32].

According to the stress waveform and energy dissipation formula of the SHPB compression test, the time history curve of energy change can be obtained as shown in Figure 14 ($p = 0.3$ MPa).

It can be seen from Figure 15 that in the initial stage of dynamic compression of limestone specimens, each energy value increases with time and gradually stabilizes after reaching a certain moment [33]. The total loading time of the incident stress wave is about 150 μS, and the loading time of the transmitted stress wave is about 120 μS. After this time, the incident energy no longer increases and the variation trend of remaining energy is also approximately horizontal.

It can also be seen from Figure 15 that the reflected energy is much greater than the transmitted energy, which is due to the close contact between the specimen and the cross-section of the pressure bar, which causes the end effect to occur. When the incident stress wave reaches the specimen cross-section, most of the incident energy is reflected back through the incident bar, except for the large amount of energy absorbed by the deformation and destruction of the specimen and only a small amount of energy is transmitted by the transmission bar.

Eight kinds of loading pressures were used to perform SHPB compression tests on saturated limestone specimens at different rates. The relationship among reflected, transmitted, and absorbed energy and incident energy is shown in Figure 14.

It can be seen from Figure 15 that when the incident energy increases, the remaining energies tend to increase. Absorptivity and transmittance both increase with the increase of incident energy, while reflectivity decreases with the increase of incident energy. Before the incident energy is 97.53 J, the reflected energy is greater than the absorbed energy, indicating that when the air pressure is low, most of the energy is emitted by the reflected wave. When the incident energy is greater than 97.53 J, the energy dissipation is mainly determined by the energy absorbed by the rock specimen. Because the rock specimen has undergone 100 freeze-thaw cycles, in the case of large initial damage, with the incident energy increased, the degree of fragmentation

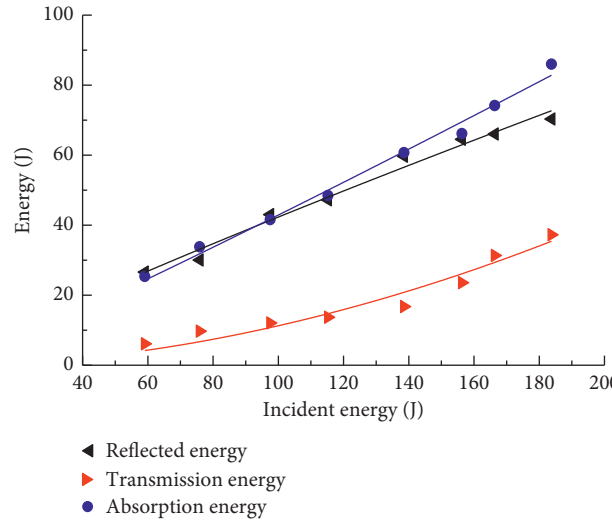

Figure 14: The relationship among reflection, transmission, absorption energy, and incident energy.

increases and the transmittance increases. As mentioned above, the dynamic elastic modulus of the rock specimen increases with the increase of air pressure. The energy required for rock specimen fragmentation also gradually increases. The absorption rate increases as well.

4.4. Strain Rate Effect and Dynamic Compressive Strength of Rock Energy Dissipation. It can be seen from Figure 16 that the strain rate of saturated limestone has an obvious energy absorption effect, and the relationship between the increase in strain rate and the energy absorption can be expressed by a fitting formula, as shown in the following equation:

$$W_L = -0.025\dot{\varepsilon}^2 - 4.2867\dot{\varepsilon} - 4.98. \tag{15}$$

Correlation coefficient (R^2) is 0.9635. With the increase of absorbed energy, the energy transfer speed inside the rock specimen is accelerated, and the strain of the rock specimen per unit time increases. But because the cracks in the saturated limestone did not expand or penetrate in time, the deformation of the specimen is lagged, resulting in the strain rate of the rock specimen increasing more and more slowly.

The relationship between dynamic compressive strength and energy absorption of saturated limestone is shown in Figure 17.

It can be seen from Figure 17 that the dynamic compressive strength increases as a function of power as the absorbed energy increases and its fitting relationship is shown in the following equation:

$$\sigma_d = 10.7986\left(W_L\right)^{0.495}. \tag{16}$$

The correlation coefficient (R^2) is 0.96689. This is due to the deformation hysteresis of the specimen as the absorbed energy increases [34]. The pore water inside the saturated rock sample has no time to affect the original cracks and new cracks, which leads to the growth rate of cracks lagging the increase rate of energy absorption, resulting in the strengthening of the dynamic strength of the rock specimen.

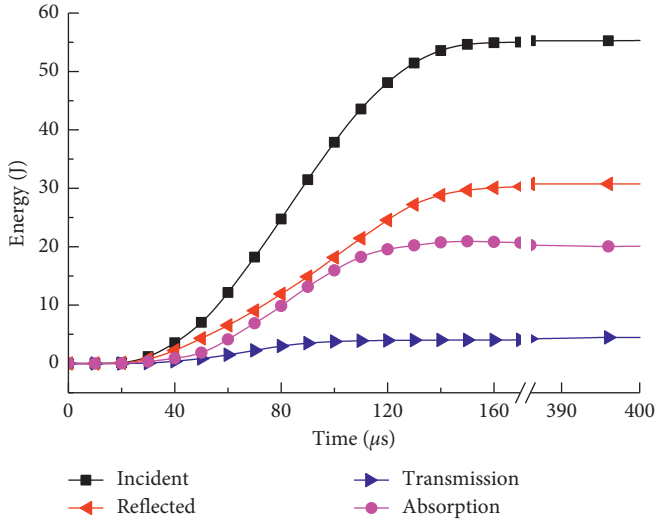

Figure 15: Time history curve of energy change of SHPB compression test of limestone specimen.

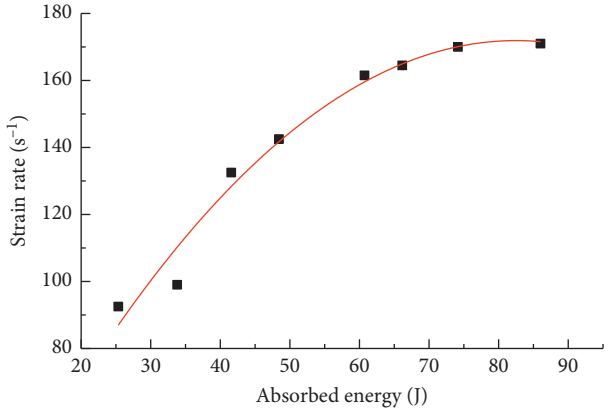

Figure 16: Relation curve between absorbed energy and the average strain rate.

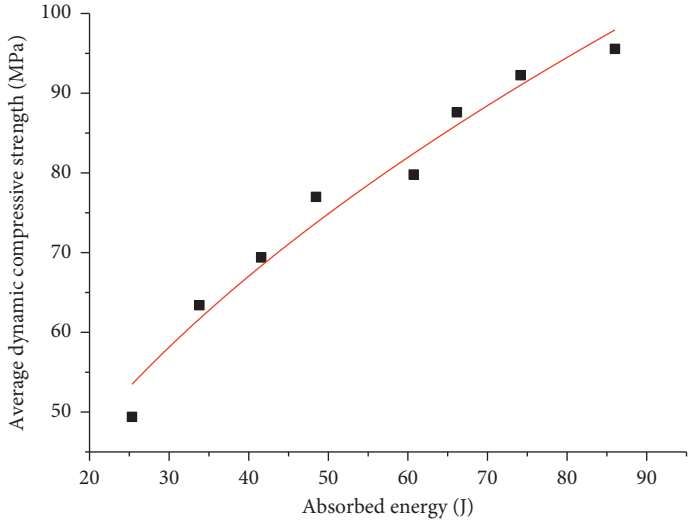

Figure 17: Relationship curve between dynamic compressive strength and absorbed energy.

When the absorbed energy is too much, the elastic strain energy inside the rock sample gradually decreases, and with the dissipated energy gradually increasing, the strength of the rock sample gradually weakens [35]. The lag at this time is negligible, which causes the trend increase of dynamic compressive strength to become smaller.

5. Conclusion

(1) The average saturation mass increase rate of rock specimens shows a continuous growth trend, but the growth rate gradually decreases. The average volume change rate of the rock specimen continued to decrease, and the decrease rate first decreased and then increased. The wave velocity of the longitudinal wave of the rock specimen continues to decline, and the rate of change of the decrease gradually becomes smaller.

(2) As the impact pressure increases, the elastic modulus of the rock specimen has an obvious strain rate effect, showing an increasing trend of decreasing growth rate. In the initial stage, due to the small impact pressure, most of the energy is reflected, resulting in the reflection energy being greater than the absorption energy. As the incident energy increases, the degree of rock specimen fragmentation increases and the transmittance increases. The dynamic elastic modulus of the rock specimen increases with the increase of impact pressure, so the energy required for rock specimen fragmentation also gradually increases and the absorption energy increases.

(3) As the absorption energy increases, the average strain rate and dynamic strength of the rock specimen increase, but the growth rate continues to decrease. While the dissipated energy gradually increases, the strength of the rock specimen gradually weakens.

Data Availability

The datasets generated and analyzed during the current study are available from the corresponding author upon reasonable request.

Conflicts of Interest

The authors declare that there are no conflicts of interest regarding the publication of this paper.

Acknowledgments

This research receives financial supports from the National Natural Science Foundation of China (No. 51674008), the Anhui Provincial Natural Science Foundation (No. 1808085ME134), the Anhui Postdoctoral Science Foundation (No. 2015B058), and the National College Student Innovation and Entrepreneurship Training Program (No. 201910361024). Thanks to the Engineering Research Center of Underground Mine Construction, Ministry of Education, Anhui University of Science & Technology, and State Key Laboratory of Mining Response and Disaster Prevention and Control in Deep Coal Mine, for providing the experiment conditions.

References

[1] R. Shi, Z. Xu, D. R. Liu, D. J. Jiang, and X. Wang, "Field measurement and analysis of ground temperature field of positive temperature gas pipeline in permafrost," *Glacial Frozen Soil*, vol. 41, no. 4, pp. 865–874, 2019.

[2] Y. Wang, H. Zhang, H. Lin, Y. Zhao, and Y. Liu, "Fracture behaviour of central-flawed rock plate under uniaxial compression," *Theoretical and Applied Fracture Mechanics*, vol. 106, p. 102503, 2020.

[3] H. Lin, H. Yang, Y. Wang, Y. Zhao, and R. Cao, "Determination of the stress field and crack initiation angle of an open flaw tip under uniaxial compression," *Theoretical and Applied Fracture Mechanics*, vol. 104, Article ID 102358, 2019.

[4] Y. Shen, Y. Wang, Y. Yang, Q. Sun, T. Luo, and H. Zhang, "Influence of surface roughness and hydrophilicity on bonding strength of concrete-rock interface," *Construction and Building Materials*, vol. 213, pp. 156–166, 2019.

[5] J. Park, C.-U. Hyun, and H.-D. Park, "Changes in microstructure and physical properties of rocks caused by artificial freeze-thaw action," *Bulletin of Engineering Geology and the Environment*, vol. 74, no. 2, pp. 555–565, 2015.

[6] G. Khanlari and Y. Abdilor, "Influence of wet-dry, freeze-thaw, and heat-cool cycles on the physical and mechanical properties of Upper Red sandstones in central Iran," *Bulletin of Engineering Geology and the Environment*, vol. 74, no. 4, pp. 1287–1300, 2015.

[7] J. Martínez-Martínez, D. Benavente, M. Gomez-Heras, L. Marco-Castaño, and M. Á. García-del-Cura, "Non-linear decay of building stones during freeze-thaw weathering processes," *Construction and Building Materials*, vol. 38, pp. 443–454, 2013.

[8] H. Deng, S. Yu, J. Deng, B. Ke, and F. Bin, "Experimental investigation on energy mechanism of freezing-thawing treated sandstone under uniaxial static compression," *KSCE Journal of Civil Engineering*, vol. 23, no. 5, pp. 2074–2082, 2019.

[9] T. Liu, C. Zhang, P. Cao, and K. Zhou, "Freeze-thaw damage evolution of fractured rock mass using nuclear magnetic resonance technology," *Cold Regions Science and Technology*, vol. 170, no. 2, p. 102951, 2020.

[10] N. G. Yang, K. P. Zhou, and Z. Lei, "Dynamic characteristics and damage laws of sandstone under freeze-thaw cycles," *Journal of Rock Mechanics and Engineering*, vol. 26, no. 10, pp. 2181–2187, 2016.

[11] L. Wen, X. B. Li, and Q. H. Wu, "Study on dynamic load strength of granite porphyry under freezing and thawing cycle," *Chinese Journal of Rock Mechanics and Engineering*, vol. 34, pp. 1–10, 2015.

[12] H. L. Jia, Q. B. Liu, and W. Xiang, "Study on damage expansion model of saturated sandstone under freezing and thawing cycle," *Journal of Rock Mechanics and Engineering*, vol. 32, no. 2, pp. 3049–3055, 2013.

[13] G. S. Yang, Y. J. Shen, and H. L. Jia, "Multi-scale research and development of mechanical properties of rock mass damage under freezing and thawing environment," *Journal of Rock Mechanics and Engineering*, vol. 37, no. 3, pp. 545–563, 2018.

[14] Y. Shen, Y. Wang, X. Wei, H. Jia, and R. Yan, "Investigation on meso-debonding process of the sandstone-concrete

interface induced by freeze-thaw cycles using NMR technology," *Construction and Building Materials*, vol. 252, p. 118962, 2020.

[15] J. Yu, G. Y. Liu, Y. Y. Cai, J. F. Zhou, S. Y. Liu, and B. X. Tu, "Time-dependent deformation mechanism for swelling soft-rock tunnels in coal mines and its mathematical deduction," *International Journal of Geomechanics*, vol. 20, no. 3, Article ID 04019186, 2020.

[16] H. Lin, W. Xiong, and Q. Yan, "Modified formula for the tensile strength as obtained by the flattened Brazilian disk test," *Rock Mechanics and Rock Engineering*, vol. 49, no. 4, pp. 1579–1586, 2016.

[17] G. Wang, Y. Luo, X. Li, T. Liu, R. Ma, and D. Qu, "Study on dynamic mechanical properties and meso-damage mechanism of jointed rock under impact load," *Arabian Journal for Science and Engineering*, vol. 45, pp. 3863–3875, 2020.

[18] G. S. Yang and C. Q. Zhang, *Rock Mass Damage and Detection*, Shaanxi Science and Technology, Xi'an, China, 1998.

[19] H. Lin, W. Xiong, Z. Xiong, and F. Gong, "Three-dimensional effects in a flattened Brazilian disk test," *International Journal of Rock Mechanics and Mining Sciences*, vol. 74, pp. 10–14, 2015.

[20] H. M. Zhang and G. S. Yang, "Experimental study on the effects of moisture and freeze-thaw effects on mechanical properties of shale," *Journal of Wuhan University of Technology*, vol. 36, no. 2, pp. 95–99, 2014.

[21] CSRME, *Rock Dynamic Characteristics Test Procedure*, Chinese Society of Rock Mechanics and Engineering, Beijing, China, 001-2019.

[22] Q. Ping, Q. Y. Ma, and P. Yuan, "Prediction and analysis of stress equilibrium time of rock specimens in SHPB test," *Journal of Vibration and Shock*, vol. 32, no. 12, pp. 55–60, 2013.

[23] Z.-l. Zhou, Y. Zhao, Y.-h. Jiang, Y. Zou, X. Cai, and D.-y. Li, "Dynamic behavior of rock during its post failure stage in SHPB tests," *Transactions of Nonferrous Metals Society of China*, vol. 27, no. 1, pp. 184–196, 2017.

[24] A. Malik, T. Chakraborty, K. S. Rao, D. Kumar, P. Chandel, and P. Sharma, "Dynamic response of deccan trap basalt under Hopkinson bar test," *Procedia Engineering*, vol. 173, pp. 647–654, 2017.

[25] X. Y. Tian, E. G. Gao, and Y. S. Bai, "Discussion on strain rate effect and anisotropy of saturated rocks," *Chinese Journal of Rock Mechanics and Engineering*, vol. 2, no. 11, pp. 1789–1792, 2003.

[26] Z.-l. Zhou, X. Cai, Y. Zhao, L. Chen, C. Xiong, and X.-b. Li, "Strength characteristics of dry and saturated rock at different strain rates," *Transactions of Nonferrous Metals Society of China*, vol. 26, no. 7, pp. 1919–1925, 2016.

[27] S. Xie, H. Lin, Y. Chen, R. Yong, W. Xiong, and S. Du, "A damage constitutive model for shear behavior of joints based on determination of the yield point," *International Journal of Rock Mechanics and Mining Sciences*, vol. 128, p. 104269, 2020.

[28] J. Yu, X. Chen, H. Li, J.-w. Zhou, and Y.-y. Cai, "Effect of freeze-thaw cycles on mechanical properties and permeability of red sandstone under triaxial compression," *Journal of Mountain Science*, vol. 12, no. 1, pp. 218–231, 2015.

[29] H. P. Xie, R. D. Peng, and Y. Ju, "Analysis of energy dissipation in the process of rock deformation and failure," *Chinese Journal of Rock Mechanics and Engineering*, vol. 23, no. 21, pp. 3568–3570, 2004.

[30] X. B. Li, *Foundation and Application of Rock Dynamics*, Science Press, Beijing, China, 2014.

[31] Y. C. You, E. B. Li, and Y. H. Tan, "Analysis of dynamic characteristics and failure characteristics of salt rock based on energy dissipation principle," *Chinese Journal of Rock Mechanics and Engineering*, vol. 36, no. 4, pp. 843–851, 2017.

[32] Q. Ping, Q. Y. Ma, and P. Yuan, "Analysis of energy dissipation in SHPB split tensile test of rock specimen," *Journal of Mining and Safety Engineering*, vol. 30, no. 3, pp. 401–407, 2013.

[33] Q. Ma, D. Ma, and Z. Yao, "Influence of freeze-thaw cycles on dynamic compressive strength and energy distribution of soft rock specimen," *Cold Regions Science and Technology*, vol. 153, pp. 10–17, 2018.

[34] Q. Ping, X. Luo, and Q. Y. Ma, "Energy consumption characteristics of crushed sandstone specimen under impact load," *Chinese Journal of Rock Mechanics and Engineering*, vol. 34, no. 2, pp. 4197–4203, 2015.

[35] S. M. Din, Z. H. Zhao, and N. N. Wang, "Classification review of rock strength theory," *Journal of Water Resources and Architectural Engineering*, vol. 15, no. 1, pp. 95–102, 2017.